Materials Science-Poland, *Vol. 27*, *No. 3*, *2009*

Quasicrystalline phase formation in the conventionally solidified Al–Cu–Fe system

M. GÖĞEBAKAN[1*], B. AVAR[1], O. UZUN[2]

[1]Department of Physics, Faculty of Art and Science, Kahramanmaras Sutcu Imam University, Kahramanmaras 46100, Turkey

[2]Department of Physics, Faculty of Art and Science, Gaziosmanpasa University, Tokat 60240, Turkey

Structural characteristics and thermal behaviour of the conventionally solidified Al–Cu–Fe alloys with nominal compositions of $Al_{70}Cu_{20}Fe_{10}$, $Al_{65}Cu_{20}Fe_{15}$ and $Al_{63}Cu_{25}Fe_{12}$ were investigated by X-ray diffraction, scanning electron microscopy, and differential thermal analysis techniques. Results show that a single quasicrystalline phase forms in a conventionally solidified $Al_{65}Cu_{20}Fe_{15}$ alloy, being thermodynamically stable without phase transition up to the melting point. A cubic AlFe(Cu) solid solution, identified as β phase, and a cubic AlCu(Fe) solid solution, identified as τ phase, were observed with quasicrystalline phase for $Al_{63}Cu_{25}Fe_{12}$ alloy. Conventional solidification of $Al_{70}Cu_{20}Fe_{10}$ alloy does not result in quasicrystalline phase formation. However, the formation of quasicrystalline phase in conventionally solidified $Al_{70}Cu_{20}Fe_{10}$ alloy was observed after additional annealing at elevated temperature. SEM micrographs for $Al_{70}Cu_{20}Fe_{10}$ and $Al_{63}Cu_{25}Fe_{12}$ alloys after annealing at 700 °C for 4 h revealed the formation of pentagonal dodecahedrons in the quasicrystalline phase, with an edge size of about 30 μm.

Key words: *quasicrystals; conventional solidification; heat treatment, Al–Cu–Fe*

1. Introduction

Quasicrystals are a new class of materials characterized by quasi-periodic order. These materials can be manufactured by mechanical alloying, rapid or conventional solidification, physical vapour deposition and plasma processing. Quasicrystals have many attractive properties, such as high hardness [1–3], low electrical and thermal conductivities [4], low surface energy [5], accompanied by a low coefficient of friction [5, 6], reasonable oxidation and strong corrosion resistance [7], and unusual optical properties [8, 9] which have not been observed for crystalline alloys. Such proper-

*Corresponding author, e-mail: gogebakan@ksu.edu.tr or mgogebakan27@hotmail.com

ties of quasicrystalline materials have been exploited for catalyst and coating applications. So far, a number of quasicrystals have been obtained in several binary, ternary and multicomponent systems. Usually, quasicrystalline phases form in systems based on Al, Mg, Zr, Ti, Zn and Cu. As the variety of base metallic elements forming quasicrystalline phases is wide, the spectrum of alloying elements is even wider. However, the alloying elements are often toxic, not easily available or very costly. Al–Cu–Fe alloys are an exception; they are interesting due to their lack of toxicity, easy availability, and reasonable costs of purchasing their alloying elements. Therefore, in the last two decades, quasicrystalline Al–Cu–TM (TM are Fe, Co, Ni) alloy systems have been intensively studied [10–14]. Most of these alloys form metastable quasicrystals which turn irreversibly into regular crystals upon heating. It has been reported that the quasicrystal phase formed in the conventionally solidified $Al_{65}Cu_{20}Fe_{15}$ alloy is thermodynamically stable and does not undergo phase transformation up to the melting point, at 1135 K [10]. Therefore, the discovery of thermodynamically stable quasicrystalline phase in $Al_{65}Cu_{20}Fe_{15}$ alloy has opened a new avenue for its experimental investigations. After the discovery, the number of alloy systems, in which quasicrystals are formed by rapid or conventional solidification, has steadily increased. The preparation, properties, structure and application of these quasicrystalline alloys have been the main topics of interest in the field of alloy science.

The structural characteristics, morphological features and thermal behaviour of the conventionally solidified $Al_{70}Cu_{20}Fe_{10}$, $Al_{65}Cu_{20}Fe_{15}$ and $Al_{63}Cu_{25}Fe_{12}$ alloys were investigated in the present study, using X-ray diffraction (XRD), scanning electron microscopy (SEM) and differential thermal analysis (DTA) techniques.

2. Experimental

The samples in this study were obtained by a conventional solidification. Three different Al–Cu–Fe alloy ingots with nominal compositions (expressed in at. %) of $Al_{70}Cu_{20}Fe_{10}$, $Al_{65}Cu_{20}Fe_{15}$ and $Al_{63}Cu_{25}Fe_{12}$ were prepared by induction melting of appropriate proportions of 99.99% purity Al, 99.9% purity Cu and 99.9% purity Fe in a graphite crucible under an argon atmosphere. The ingots were re-melted several times in order to achieve homogeneity. Then the ingots were left to cool in air to allow slow cooling. The master ingots were annealed at 700 °C for 4 h under vacuum. phase identification and microstructural examination of as-cast and heat-treated alloy specimens were carried out using X-ray diffraction (XRD) and scanning electron microscopy (SEM). The XRD examination was performed using a Philips X`Pert PRO diffractometer with CuK_α radiation with the wavelength of 0.154 nm. For phase identification, measurements were taken for a wide range of diffraction angles (2θ) ranging from 20° to 120° with a scanning rate of 5 deg/min. SEM analysis was performed with a JEOL JSM 5400 scanning electron microscope at an acceleration voltage of 20 kV after the specimen had been coated with a vacuum-deposited gold layer in order to enhance

contrast. Thermal properties of the master ingot alloys were analysed by differential thermal analysis (DTA) using a Perkin-Elmer's Diamond TG/DTA thermal analyser at 20 K/min heating rate under flowing N_2.

3. Results and discussion

Figure 1 shows the XRD patterns for conventionally solidified $Al_{70}Cu_{20}Fe_{10}$, $Al_{65}Cu_{20}Fe_{15}$ and $Al_{63}Cu_{25}Fe_{12}$ alloys. The XRD trace of the $Al_{70}Cu_{20}Fe_{10}$ alloy (curve a) shows the presence of cubic β-AlFe(Cu) solid solution phase (β phase), tetragonal θ-Al_2Cu phase (θ phase) and a small amount of tetragonal ω-Al_7Cu_2Fe phase (ω phase).

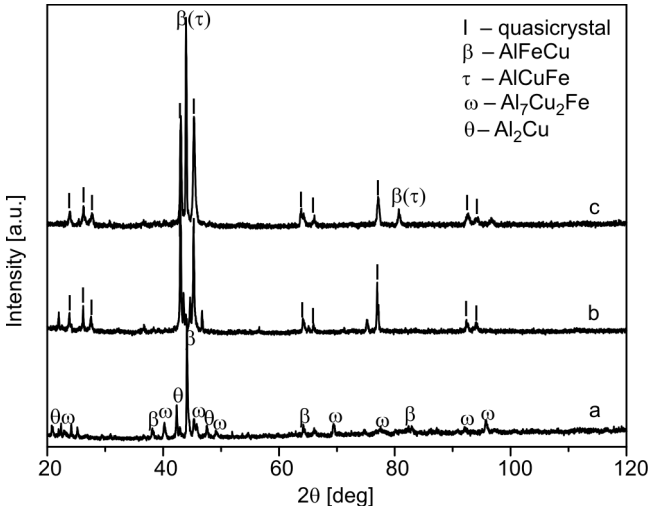

Fig. 1. XRD patterns for conventionally solidified Al–Cu–Fe alloys: a) $Al_{70}Cu_{20}Fe_{10}$, b) $Al_{65}Cu_{20}Fe_{15}$ and c) $Al_{63}Cu_{25}Fe_{12}$

It is clear from the peak intensities that β is the major phase for this alloy composition. However, the present result indicated that iron concentration in $Al_{70}Cu_{20}Fe_{10}$ alloy is too low to form quasicrystalline phase by a conventional solidification. For the $Al_{65}Cu_{20}Fe_{15}$ alloy (curve b), only the icosehedral quasicrystalline phase (I phase) was distinguished in the XRD pattern. In the XRD curve of the $Al_{63}Cu_{25}Fe_{12}$ alloy (curve c), mainly the peaks associated with I phase, the cubic β phase and cubic τ-AlCu(Fe) solid solution phase (τ phase) were observed. As shown in Fig. 1 (curve c), the diffraction peaks of τ phase exactly overlap with the diffraction peaks of β phase, owing to the same crystal structure of CsCl type cubic and a very similar lattice parameter, approximately 0.293 nm [15]. However, these results indicated that the single quasicrystalline phase is formed only in the conventionally solidified $Al_{65}Cu_{20}Fe_{15}$ alloy.

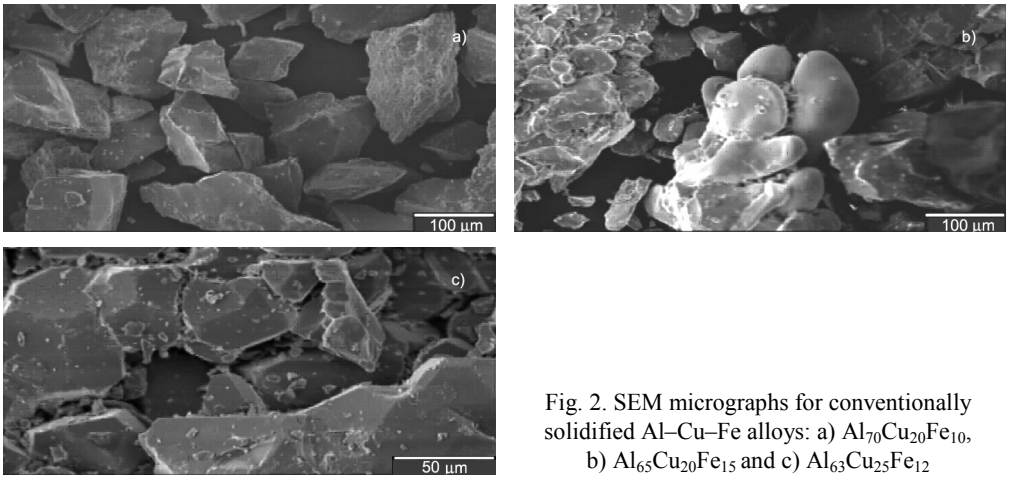

Fig. 2. SEM micrographs for conventionally solidified Al–Cu–Fe alloys: a) $Al_{70}Cu_{20}Fe_{10}$, b) $Al_{65}Cu_{20}Fe_{15}$ and c) $Al_{63}Cu_{25}Fe_{12}$

With the aim of examining the compositional dependence of the microstructure for conventionally solidified Al–Cu–Fe alloys in more detail, the alloys were also examined by SEM. Figure 2 shows the SEM micrographs for conventionally solidified $Al_{70}Cu_{20}Fe_{10}$, $Al_{65}Cu_{20}Fe_{15}$ and $Al_{63}Cu_{25}Fe_{12}$ alloys. These micrographs showed different microstructural features. For $Al_{70}Cu_{20}Fe_{10}$ alloy, no appreciable quasicrystals were observed, in agreement with the XRD results. This is probably because the composition of this alloy is very different from that of quasicrystalline phase. The morphology of this alloy is diverse and some particles exhibited faceted morphology, as shown in Fig. 2a. The SEM micrograph of the $Al_{65}Cu_{20}Fe_{15}$ alloy reveals the formation of the 'cauliflower' morphology observed in previous studies [16, 17]. The grain size of this quasicrystal ranges from 20 to 80 μm. However, for the $Al_{63}Cu_{25}Fe_{12}$ alloy, typical pentagonal dodecahedral crystals were clearly observed, as seen in Fig. 2c. Therefore, it is emphasized that a slight change in the compositions would cause a significant difference in the microstructural evolution during metallurgical processing.

In order to investigate the structural change that occurs during heat treatment of Al–Cu–Fe alloys, the samples were annealed for 4 h at 700 °C and then cooled rapidly to freeze the microstructure for subsequent XRD and SEM analysis. Figure 3 shows the XRD patterns for conventionally solidified Al–Cu–Fe alloys after annealing for 4 h at 700 °C. The XRD pattern of the $Al_{70}Cu_{20}Fe_{10}$ alloy consisted of a mixture of I, β and ω phases. Therefore, the icosahedral quasicrystalline phase (I phase) in conventionally solidified $Al_{70}Cu_{20}Fe_{10}$ alloy was observed after heat treatment at 700 °C for 4 h. At this processing stage, the peak intensity of ω phase increased.

As seen in Fig. 3b, the XRD patterns of an $Al_{65}Cu_{20}Fe_{15}$ alloy in as-solidified state and heated state at 700 °C were quite similar. No appreciable differences, even in the peak position and peak intensity, were observed in either cases. All the diffraction peaks were identified as I phase. This result clearly indicated that I phase is formed as a thermodynamically stable phase in $Al_{65}Cu_{20}Fe_{15}$ alloy. This is in good agreement with the results for the conventionally solidified $Al_{65}Cu_{20}Fe_{15}$ reported earlier by Tsai

et al. [10]. On the other hand, XRD patterns of the $Al_{63}Cu_{25}Fe_{12}$ alloy after additional annealing for 4 h at 700 °C showed a considerable increase in the diffraction intensities corresponding to I phase.

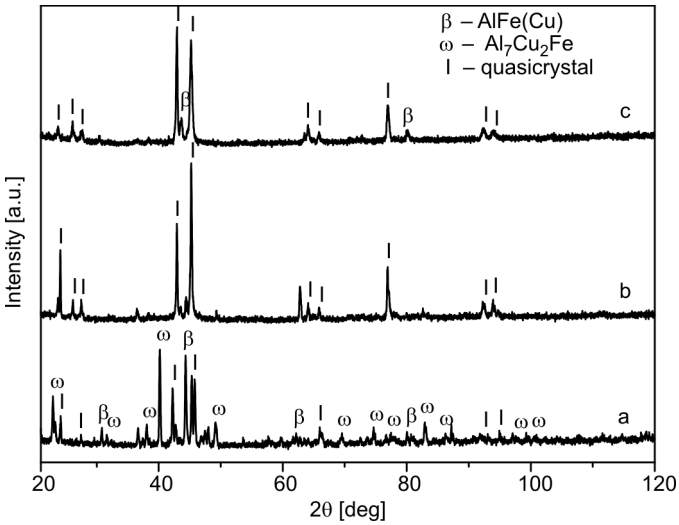

Fig. 3. XRD patterns for conventionally solidified Al–Cu–Fe alloys annealed for 4 h at 700 °C: a) $Al_{70}Cu_{20}Fe_{10}$, b) $Al_{65}Cu_{20}Fe_{15}$ and c) $Al_{63}Cu_{25}Fe_{12}$

As is seen in Fig. 3c, the τ phase completely disappears at this stage. It has been reported that the τ phase is a metastable one, containing less Fe with a lower melting temperature and the β phase is a stable phase, containing more Fe with a higher melting temperature [18]. Thus, the present investigation demonstrates that during the heat treatment of $Al_{63}Cu_{25}Fe_{12}$ alloy, the τ phase melted and peritectic reaction occurred between liquid and β phases. It is therefore reasonable to assert that the I phase in $Al_{63}Cu_{25}Fe_{12}$ alloy formed as the result of a peritectic reaction. This is in agreement with other results [15, 19, 20]. Therefore, the XRD pattern of the $Al_{63}Cu_{25}Fe_{12}$ alloy after additional annealing for 4 h at 700 °C consists of I phase and the β phase.

Figure 4 shows SEM micrographs for conventionally solidified Al–Cu–Fe alloys after additional annealing for 4 h at 700 °C. High magnification SEM results for the $Al_{70}Cu_{20}Fe_{10}$ and $Al_{63}Cu_{25}Fe_{12}$ alloys after annealing for 4 h at 700 °C revealed the formation of pentagonal dodecahedrons in the quasicrystalline phase with the edge size of about 30 μm as shown in Fig. 4a and c. The icosahedral quasicrystal particles, in the shape of dodecahedrons, for conventionally solidified Al–Cu–Fe alloy have been previously reported [10, 15, 21]. However, the SEM micrograph of $Al_{65}Cu_{20}Fe_{15}$ alloy after annealing for 4h at 700 °C shows an array of the pentagonal dodecahedral crystals in the shape of a cauliflower, as seen in Fig. 4b. Therefore the SEM micrographs of $Al_{65}Cu_{20}Fe_{15}$ alloy in as-solidified state and after heat treatment, at 700 °C for 4 h, were quite similar.

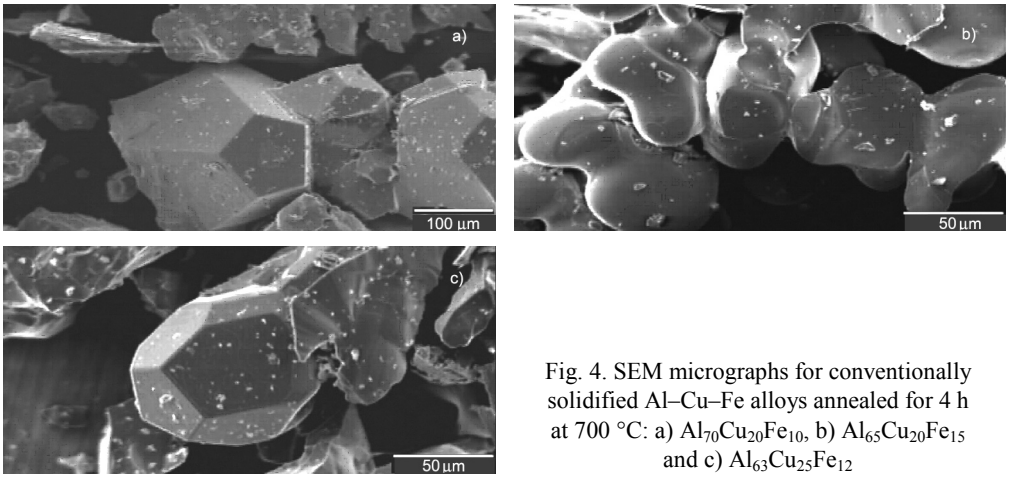

Fig. 4. SEM micrographs for conventionally solidified Al–Cu–Fe alloys annealed for 4 h at 700 °C: a) $Al_{70}Cu_{20}Fe_{10}$, b) $Al_{65}Cu_{20}Fe_{15}$ and c) $Al_{63}Cu_{25}Fe_{12}$

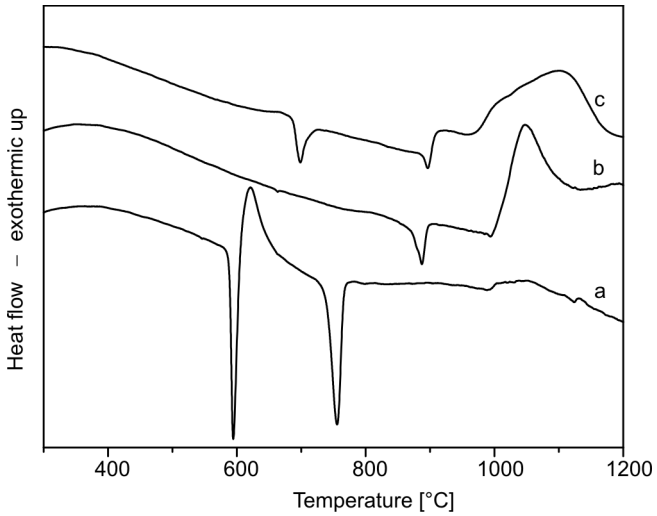

Fig. 5. DTA curves for conventionally solidified Al–Cu–Fe alloys: a) $Al_{70}Cu_{20}Fe_{10}$, b) $Al_{65}Cu_{20}Fe_{15}$ and c) $Al_{63}Cu_{25}Fe_{12}$ alloy

Figure 5 shows the DTA curves for conventionally solidified $Al_{70}Cu_{20}Fe_{10}$, $Al_{65}Cu_{20}Fe_{15}$ and $Al_{63}Cu_{25}Fe_{12}$ alloys. The DTA traces for $Al_{70}Cu_{20}Fe_{10}$ alloy showed two major endothermic peaks at around 595 °C and 750 °C, respectively, during heating up to 1200 °C. The pseudo-binary Al_3Fe–Al_2Cu phase diagram indicated that the melting points of θ and ω phases are 591°C and 740 °C, respectively [22]. Thus, it is clear that the endothermic peaks around 595 °C and 750 °C correspond to the melting of the θ phase and ω phase. In addition, the DTA traces of the $Al_{70}Cu_{20}Fe_{10}$ alloy also showed an exothermic effect at around 615 °C. This exothermic effect is attributed to formation of the ω phase. This result is consistent with XRD observation. As men-

tioned above, the XRD patterns of the $Al_{70}Cu_{20}Fe_{10}$ alloy indicated the presence of the β and θ phases, a small amount of ω phase, and after the sample had been heated to 700 °C for 4 h, the peak intensity of the ω phase increased.

On the other hand, the DTA curve of the $Al_{65}Cu_{20}Fe_{15}$ alloy showed only one endothermic peak, around 890 °C, corresponding to the fusion. This result indicated that the quasicrystal has a melting point at 890 °C, and is a stable phase without phase transition up to the melting point. Furthermore, the endothermic peak corresponding to the fusion takes places at a single stage; no splitting in the peak was observed, indicating that the $Al_{65}Cu_{20}Fe_{15}$ quasicrystal is mostly composed of a single phase. This is again consistent with XRD results, since XRD patterns of the $Al_{65}Cu_{20}Fe_{15}$ alloy annealed up to 700 °C for 4 h showed no significant difference, even in the peak position and peak intensity. However, this DTA result is quite similar to the earlier one reported for the $Al_{65}Cu_{20}Fe_{15}$ by Tsai et al. [10]. The DTA trace of $Al_{63}Cu_{25}Fe_{12}$ alloy shows mainly two endothermic peaks at around 700 °C and 896 °C, respectively. The first endothermic peak at around 700 °C is considered to correspond to the dissolution of the τ phase. This observation is consistent with the conclusion obtained from Fig. 3c, where no τ phase was observed after the sample had been heated to 700 °C for 4 h. The second endothermic peak at around 896 °C corresponds to the melting of I phase.

4. Conclusions

In the present study, the formation of icosahedral quasicrystalline phase in conventionally solidified Al–Cu–Fe alloys has been investigated.

The microstructure of the as-solidified $Al_{70}Cu_{20}Fe_{10}$ alloy consisted of a mixture of β, θ and ω phases. However, for this alloy, the formation of the I phase was observed after additional annealing at elevated temperatures. A single quasicrystalline phase was observed in the conventionally solidified and annealed $Al_{65}Cu_{20}Fe_{15}$ alloy.

SEM micrographs of this alloy in as-solidified state and after heat treatment at 700 °C for 4 h, showed an array of the pentagonal dodecahedral crystals in the shape of a cauliflower.

The DTA curve of the $Al_{65}Cu_{20}Fe_{15}$ alloy showed only one endothermic peak around 890 °C corresponding to the fusion. The DTA result indicated that the $Al_{65}Cu_{20}Fe_{15}$ quasicrystal is mostly composed of a single phase, and is a thermodynamically stable phase without phase transition up to melting point.

As-solidified $Al_{63}Cu_{25}Fe_{12}$ alloy exhibited I phase together with β phase and τ phase. After annealing at 700 °C for 4 h, the τ phase completely disappeared and the sample consisted of I phase and β phase.

SEM micrographs for the $Al_{70}Cu_{20}Fe_{10}$ and $Al_{63}Cu_{25}Fe_{12}$ alloys annealed for 4 h at 700 °C revealed the formation of pentagonal dodecahedrons in the quasicrystalline phase.

Acknowledgements

This work was supported by The Scientific and Technological Research Council of Turkey (TUBITAK), Project No. 106 T 701.

References

[1] KOSTER U., LIU W., HERTZBERG H.,, MICHEL M., J. Non-Cryst. Solids,153/154 (1993), 446.
[2] WOLF B., BAMBAUER K.O., PAUFLER P., Mater. Sci. Eng. A, 298 (2001), 284.
[3] HUTTUNEN-SAARIVIRTA E., J. Alloys Compds. 363 (2004), 150.
[4] RAPP O., Mater. Sci. Eng. A, 294–296 (2000), 458.
[5] DUBOIS J.M., Mater. Sci. Eng. A, 294–296 (2000), 4.
[6] BRUNET P., ZHANG L.M., SORDELET D.J., BESSER M., DUBOIS J.M., Mater. Sci. Eng. A, 294–296 (2000), 74.
[7] CHANG S.L., CHIN W.B., ZHANG C.M., JENKS C.J., THIEL P.A., Surf. Sci., 337 (1995), 135.
[8] HOMES C.C., TIMUSK T., WU X., ALTOUNIAN Z., SAHNOUNE A., STROM-OSLEN J.O., Phys. Rev. Lett., 13 (1991), 2694.
[9] EISENHAMMER T., MAHR A., HAUGENEDER A., ASSMANN W., Sol. Energy Mater. Sol. Cells, 46 (1997), 53.
[10] TSAI A.P., INOUE A., MASUMOTO T., Japan. J. Appl. Phys., 26 (1987), L1505.
[11] BOJARSKI Z., BOGDANOWICZ W., Arch. Nauk. Mater., 19 (1998), 215.
[12] BOJARSKI Z., BOGDANOWICZ W., GIGLA M., LELATKO J., SUROWIEC M., Arch. Nauk. Mater., 18 (1997), 237.
[13] BOGDANOWICZ W., J. Cryst. Growth, 240 (2002), 255.
[14] BOGDANOWICZ W., Mater. Sci. Eng. A, 346 (2003), 328.
[15] LEE S.M., KIM B.H., KIM S.H., FLEURY E., KIM W.T., KIM D.H., Mater. Sci. Eng. A, 294–296 (2000), 93.
[16] CHEUNG Y.L, CHAN K.C., ZHU Y.H., Mater. Charact., 47 (2001), 299.
[17] ROSAS G., REYES-GASGA J., PEREZ R., Mater. Charact., 58 (2007), 765.
[18] KIM B.H., KIM S.H., KIM W.T., KIM D.H., Phil. Mag. Lett., 81 (2001), 483.
[19] LEE S.M., KIM W.T., KIM D.H., Mater. Sci. Eng. A, 294–296 (2000), 99.
[20] LEE S.M., JEON H.J., KIM B.H., KIM W.T., KIM D.H., Mater. Sci. Eng. A, 304–306 (2001), 871.
[21] HOLLAND-MORITZ D.,SCHROERS J., GRUSHKO B., HERLACH D.M.,, URBAN K., Mater. Sci. Eng. A, 226–228 (1997), 976.
[22] FAUDOT F., QUIVY A., CALVAYRAC Y., GRATIAS D., HARMELIN M., Mater. Sci. Eng. A 133 (1991), 383.

Received 17 October 2008
Revised 5 December 2008